www.MaterialsViews.com

Controlling the Visible Electromagnetic Resonances of Si/SiO_2 Dielectric Core–Shell Nanoparticles by Thermal Oxidation

Yuta Tsuchimoto, Taka-aki Yano, Masaki Hada, Kazutaka G. Nakamura, Tomohiro Hayashi, and Masahiko Hara*

Dielectric nanostructures with a high refractive index and a low optical loss have attracted considerable attention as an alternative to plasmonic nanostructures. Electromagnetic multipoles excited in the high-index dielectric nanostructures enable us to the manipulation of light beyond the diffraction limit and to offer high electromagnetic field enhancement comparable with that exhibited by the plasmonic nanostructures. In addition, these nanostructures have the remarkable advantage of being able to suppress heat generation caused by energy losses and quenching.[1,2] Recently numerical calculations have demonstrated that dielectric nanoantennas made of gallium phosphide exhibit ultra-low energy losses with strongly enhanced electromagnetic fields in the visible region.[1] An analytical model based on dipole–dipole interactions has demonstrated that nanodimmers made of silicon (Si) produce strongly localized electromagnetic field and show a high quantum efficiency of localized emitters while suppressing quenching.[2] These results are promising for the applications of dielectric nanostructures in field-enhanced spectroscopy and imaging.

Dielectric nanoparticles have been also considered as a good magnetic resource for the metamaterials working in the visible spectral region. They are known to possess both electric dipole (ED) and also magnetic dipole (MD) resonances in the visible region.[3–6] MDs are excited in the nanoparticles through circulating displacement currents generated inside the particles, and they scatter the "magnetic" light into far-field. Fundamental characteristics of the dielectric nanostructures as a magnetic resource have been experimentally[3,5,7] and theoretically[8,9] studied. Using theoretical analysis based on Mie theory, Si nanoparticles have been shown to exhibit MD resonances in the visible[4] and infrared[8] regions, that are strongly dependent on the nanoparticle size. Strong MD responses of Si nanoparticles were experimentally observed in the visible region of the spectrum with the use of a dark-field optical microscope.[3,5] Along with the far-field studies, the near-field characteristics of localized magnetic fields of silicon dimmers have been investigated; in these, hot spots derived from MDs were visualized with the use of near-field scanning optical microscopy.[10]

EDs and MDs excited in the dielectric nanostructures lead to attractive scattering properties enabling us to achieve unidirectional scattering.[11–15] In 1983, Kerker et al. theoretically demonstrated that dielectric particles exhibit spatially anisotropic scattering patterns arising from interference of EDs and MDs inside the particles.[16] The theory predicted complete suppression of back scattering light from magnetodielectric particles that have recently been experimentally verified in the visible spectra region using Si and gallium arsenide nanoparticles.[11,12]

Resonant wavelengths of electric and magnetic multipoles can be controlled by the shapes of dielectric nanostructures, leading to tunability of spectral distances of the optical resonances.[17,18] Laser printing of single Si nanoparticles, which enables control of particle size and arrangement of complex structures precisely, has been developed recently.[19] Among the dielectric nanostructures with various shapes, core–shell nanoparticles may open up a novel way of controlling the optical properties mentioned above because of their tunability of electromagnetic resonances and scattering directivity. Recently, several theoretical studies have been

Y. Tsuchimoto, Dr. T. Yano, Prof. T. Hayashi, Prof. M. Hara
Department of Electronic Chemistry
Tokyo Institute of Technology
Yokohama, Kanagawa 226-8503, Japan
E-mail: yano@echem.titech.ac.jp
Dr. T. Yano, Prof. T. Hayashi, Prof. M. Hara
RIKEN
2-1 Hirosawa
Wako, Saitama 351-0198, Japan
Dr. M. Hada, Prof. K. G. Nakamura
Materials and Structures Laboratory
Tokyo Institute of Technology
Nagatsuta 4259, Yokohama 226-8503, Japan
Dr. M. Hada
PRESTO
Japan Science and Technology Agency
Kawaguchi 332-0012, Japan
Prof. K. G. Nakamura
CREST
Japan Science and Technology Agency
Kawaguchi 332-0012, Japan
Prof. M. Hara
Earth-Life Science Institute
Tokyo Institute of Technology
Meguro, Tokyo 152-8551, Japan

DOI: 10.1002/smll.201500884

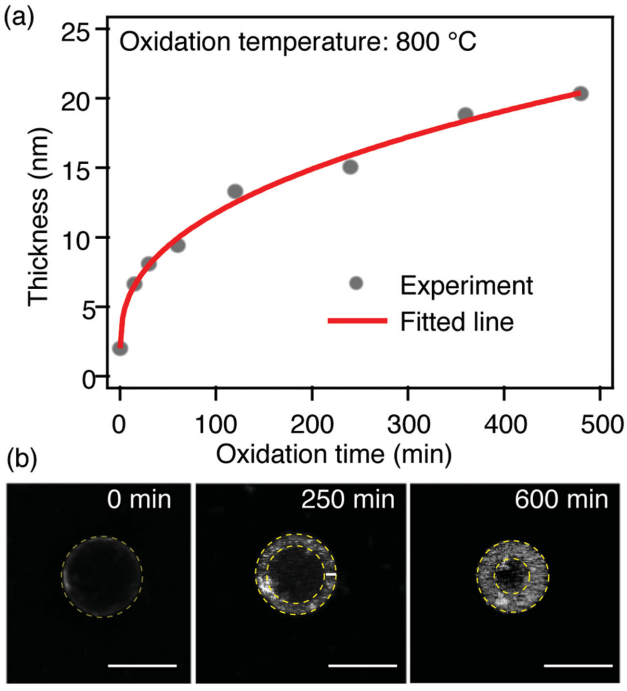

Figure 1. (a) Relation between oxidation time and thickness of SiO_2 layer on Si substrate measured using an ellipsometer. (b) SEM images of Si/SiO_2 nanoparticles obtained at various oxidation times. Yellow dashed lines indicate boundaries between the Si core and SiO_2 shell. The scale bars correspond to 100 nm.

performed focusing on the directivity.[20–22] For instance, core–shell nanoparticles composed of metal and dielectric material have been found to suppress backward scattering and enhance forward scattering.[20] Such directional control of scattering has also been theoretically demonstrated by all dielectric core–shell spheres with macroscopic sizes.[21]

In this paper, we demonstrate the control of the optical resonances of dielectric core–shell nanoparticles made of Si and silicon dioxide (SiO_2), and investigate their optical properties in the visible region through experimental far-field observations and calculations using the finite element method (FEM) and Mie theory. Strong electromagnetic resonances exhibited by the core–shell nanoparticles are easily controlled by changing the core diameter using simple thermal oxidation. The near-field characteristics of the core–shell nanoparticles are also elucidated.

As a preliminary experiment for the fabrication of Si/SiO_2 (core/shell) nanoparticles, the relation between the thermal oxidation time and the thickness of a SiO_2 layer on a Si substrate was obtained. Thermal oxidation of Si substrates was performed under dry air conditions in an electric furnace at a constant temperature of 800 °C with various oxidation times. The thicknesses of the SiO_2 layers on the substrates were then measured by an ellipsometer. **Figure 1**a describes the relation between the oxidation time and thickness. Gray points and the red line show the experimentally obtained thicknesses and a fit by a power function, respectively. The experimental conditions enabled the thermal oxidation to proceed slowly with time, allowing us to easily control the thickness of the oxidized SiO_2 layer on Si. We have confirmed that the oxidation temperatures of 900 °C and 1000 °C are too high to control the SiO_2 thickness within the range of several nanometers due to thier high oxidation velocities. The optimized conditions of the oxidation time and temperature were then applied for the oxidation of Si nanoparticles prepared by the laser-ablation method (see Experimental Section for details). Figure 1b shows the scanning electron microscope (SEM) images of the Si/SiO_2 nanoparticles on a Si substrate fabricated using different oxidation times that were taken at the accelerating voltage of 15 kV. Brighter regions inside the particles are interpreted as SiO_2 shells while the darker ones are Si cores; this is due to a secondary electron emission yield of SiO_2 compared with than that of Si.[23,24] This result indicates the formation of the oxidized SiO_2 layers on the surfaces of Si nanoparticles. The SiO_2 shell layers expanded from the outermost edge of the particles into the inside with increasing thermal oxidation time. These results verified that the core–shell ratio was controlled on the nanometer scale by the thermal oxidation time.

Forward scattering spectra of a Si/SiO_2 nanoparticle prepared on a quartz substrate were investigated as the Si/SiO_2 ratio was changed by the thermal oxidation. **Figure 2**a shows an SEM image taken at the accelerating voltage of 5 kV, confirming that the particle diameter was approximately 155 nm. Figure 2b–g show dark-field images of the same particle obtained using various oxidation times of 0, 15, 30, 60, 120,

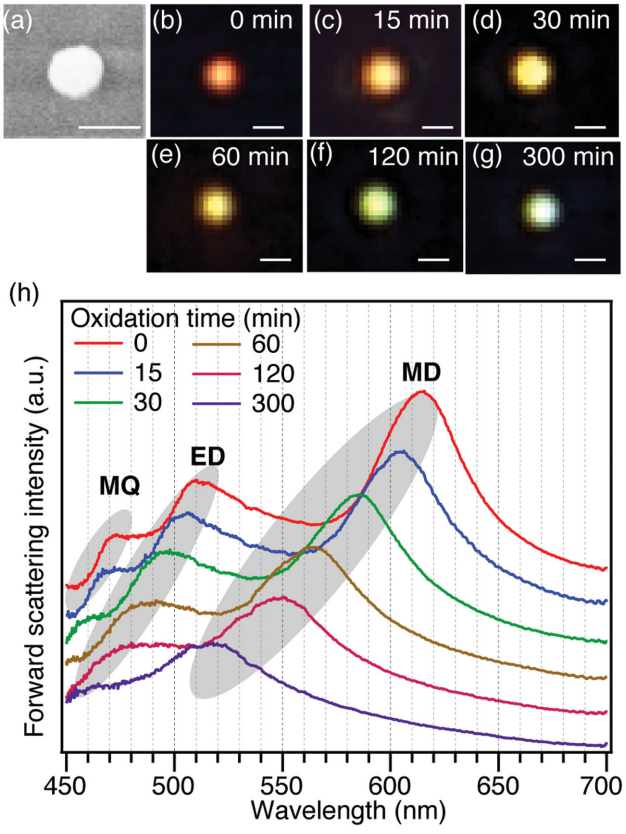

Figure 2. (a) An SEM image of an as-fabricated Si nanoparticle on quartz substrate. The scale bar corresponds to 100 nm. (b–g) dark-field images of the same Si/SiO_2 nanoparticle obtained at various oxidation times. The scale bars correspond to 500 nm. (h) Experimentally obtained forward scattering spectra of the nanoparticles shown in (a).

www.MaterialsViews.com

and 300 min, respectively. The color of the particle changed drastically from red to green with the increase of the oxidation time, corresponding to a decrease in the core diameter or an increase in the shell thickness. The scattering spectra of the Si/SiO_2 nanoparticle obtained with the various oxidation times were presented in Figure 2h. In each spectrum, the large peak located at the longer wavelength side and small peak at the shorter wavelengths are attributed to the MD and ED resonances, respectively.[3,5] An additional peak that appears next to the ED resonances is derived from magnetic quadrupoles (MQ).[3,5] Since the MD resonances are the strongest in all spectra, the colors observed in Figure 2b–g originate from forward scattering of the MD resonances. All the resonant peaks observed in each spectrum show a distinct blue shift within the visible region with the increase of the oxidation time. Since the MDs and EDs were clearly excited for all of the Si/SiO_2 nanoparticles with different core/shell ratios, the Si/SiO_2 nanoparticles appear to behave as a good resource of the resonances and exhibit the desired controllability of the electromagnetic resonances in the visible region.

To analyze the scattering spectra in Figure 2h, we calculated the forward scattering cross sections in the visible region for a Si/SiO_2 nanoparticle with the fixed total diameter of 155 nm and the diameter of the Si core varied from 151 to 95 nm, corresponding to the variation of the SiO_2 layer thickness from 2 to 30 nm. In this calculation, a native oxide layer was assumed to be 2 nm corresponding to that on the Si substrate shown in Figure 1a. Since the experimental spectrum at the oxidation time of 0 min shows good agreement with the calculated one using the dielectric constant of crystalline Si rather than amorphous one (see Figure S1, Supporting Information), the Si nanoparticles fabricated by the laser-ablation method were regarded as crystals. **Figure 3** shows a waterfall plot for the forward scattering spectra calculated as a function of the core diameter. Two intense bands originating from the ED and MD resonances are observed in the waterfall plot; these exhibit the blue-shift and decrease of the scattering intensity with decreasing core diameter for both resonances. The calculated spectra were in fairly good agreement

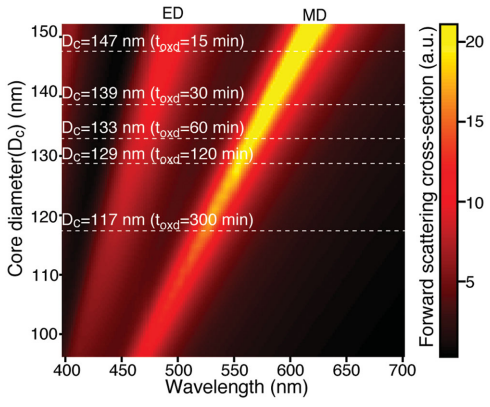

Figure 3. Calculated forward scattering cross-sections of a Si/SiO_2 nanoparticle with the fixed total diameter of 155 nm and variation of core diameter from 95 to 151 nm. White dashed lines show the calculated spectra that are in the best agreement with the experimentally obtained spectra shown in Figure 2(h). Corresponding core diameter and thermal oxidation times are written above the each line.

with the experimental scattering spectra shown in Figure 2h. The slight discrepancy between the experimental and the calculated ED resonance peak positions is due to the "dressing effect."[5,11] Here, five dashed lines drawn in Figure 3 indicate the scattering spectra for which the MD resonances are in best agreement with experimental data shown in Figure 2h. According to the waterfall plot, the five lines (spectra) correspond to the Si/SiO_2 nanoparticles with the core diameters of 147, 139, 133, 129, and 117 nm. The shell thicknesses of the five particles are in good agreement with those of the particles experimentally fabricated using different oxidation times (t_{oxid}), as estimated from the relationship in Figure 1a. The agreement between experimental and theoretical results verified that the blue shift shown in Figure 2h originated from the decrease of the core diameter or the increase of the shell thickness through the thermal oxidation.

To examine the contribution of the core and the shell to the spectral shift observed in Figure 2h and Figure 3, two types (Type 1 and Type 2) of Si nanostructures are first modeled. Type 1 is a Si/SiO_2 nanoparticle with fixed total diameter of 155 nm while Type 2 is a bare Si core nanoparticle. The forward scattering spectra of both types were calculated as a function of diameters of the Si cores and compared so as to estimate influence of the core, which are shown in **Figure 4**a. The resonant wavelengths of the MD and ED for Type 2 exhibit similar behavior to those for Type 1. The maximum difference of the resonant wavelengths is only 10 nm in the wide 95–151 nm range of the examined Si core diameters. Second, to estimate influence of the shell, we calculated resonant wavelengths of a Si/SiO_2 nanoparticle with the fixed core diameter of 120 nm and with various shell thicknesses (Type 3). Figure 4b shows the shell thickness dependence of the resonant wavelengths of Type3. Even though the shell thickness varied strongly from 0 to 40 nm, the MD and ED resonant wavelengths are shifted by only ≈10 nm. Therefore, the experimentally observed drastic blue shift of the resonant wavelengths (Figure 2h) is mainly caused by the change of the Si core diameter rather than the change of the SiO_2 shell thickness. It should be additionally noted that the shell thickness would affect the resonant wavelengths only when the refractive index of the shell is much higher than that of the SiO_2 shell utilized in our experiments as shown in Figure S2 (Supporting Information).

In general, there are two factors that can induce difference of optical resonances between a bare Si and a Si/SiO_2 nanoparticle. One is the size of a Si core that has already been shown in Figure 4a. The other one is the refractive index of a surrounding medium. Here, for both nanoparticles, we discuss influence of refractive index change of a surrounding medium on the MD and ED resonant wavelengths using Mie coefficients. In this analytical calculation, the core diameter and shell thickness of the Si/SiO_2 nanoparticle were set to be 120 and 17.5 nm while the diameter of the bare Si nanoparticle was assumed to be 155 nm, resulting in the same total diameter for both nanoparticles. The MD and ED resonant wavelengths of those nanoparticles are calculated over the practical refractive index range of 1.0–1.6 as shown in **Figure 5**. The ED resonant wavelength of the bare Si nanoparticle shows remarkable red shift of ≈40 nm with

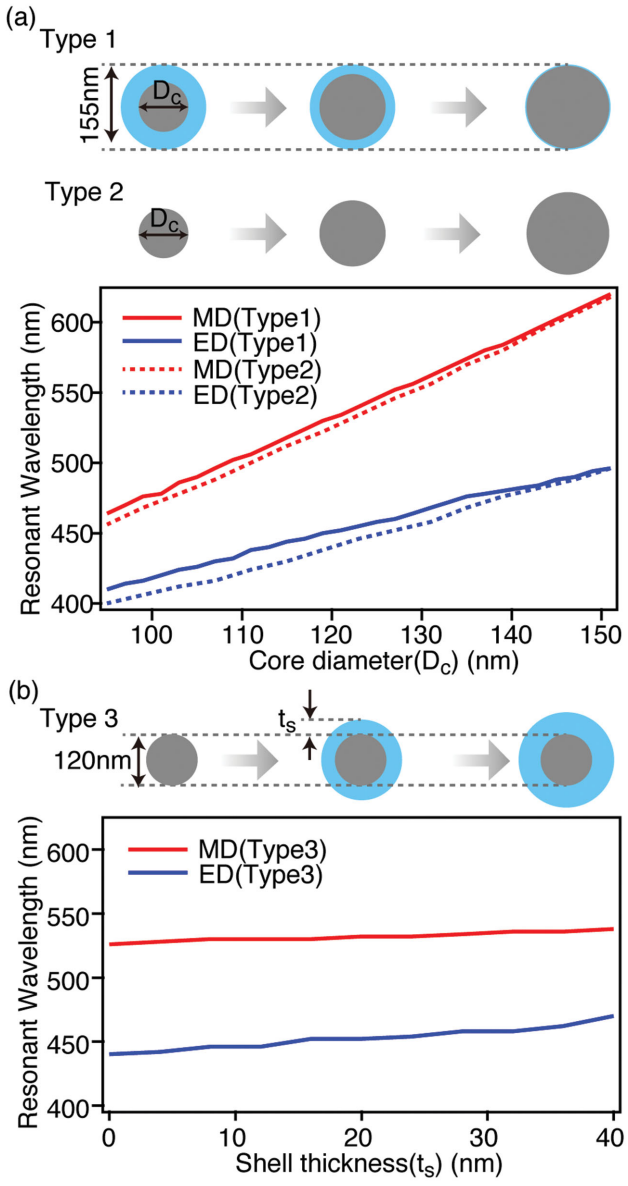

Figure 4. Comparison of resonant wavelengths between Si/SiO_2 nanoparticle (Type 1) with fixed diameter of 155 nm and bare Si core (Type 2) with various core diameters. (b) Shell thickness dependence of the resonant wavelengths of the Si/SiO_2 nanoparticle (Type 3) with the fixed core diameter of 120 nm and various shell thicknesses.

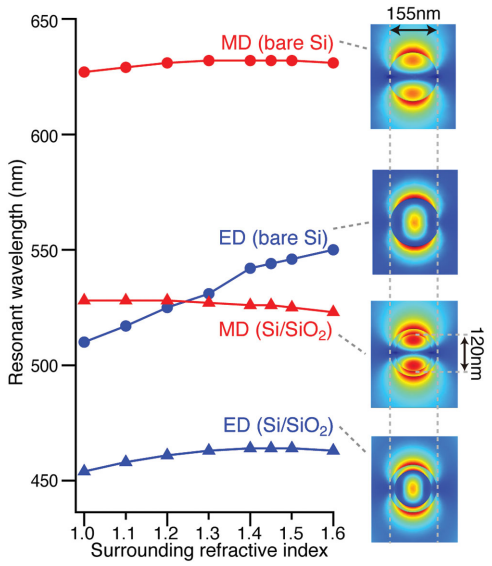

Figure 5. Calculated resonant wavelengths of MDs and EDs for a bare Si nanoparticle (diameter: 155 nm) and a Si/SiO_2 nanoparticle (core diameter: 120 nm, shell thickness: 17.5 nm) using Mie coefficients. The insets show electric near-field intensity distributions of those nanoparticles at MD and ED resonances.

increasing the refractive index of the surrounding medium in contrast to the all other resonances of which wavelength shifts are about 9 nm. The difference results from the electric near-field distributions at each resonance (see the insets in Figure 5). In the case of the ED resonance of the bare Si nanoparticle, the induced near field extends to the surrounding medium, which leads to the large wavelength shift in response to the change of the refractive index.[25–27] On the other hands, the strong near fields concentrate inside the nanoparticles at the all other dipole resonances. Namely, in the case of the ED resonance of the Si/SiO_2 nanoparticle, the SiO_2 shell confines large amount of the near field into the Si/SiO_2 nanoparticle, resulting in the little wavelength shift. For the MD resonances of both nanoparticles, the electric near fields of MDs are intrinsically localized inside the nanoparticles, and hence the MD resonances are not affected by the surrounding medium.[25–27] To quantitatively analyze the near-field effect, we also calculated energy ratios of electric near fields outside the nanoparticles (i.e., leaked into the surrounding medium) to the total electric near fields inside and outside of the nanoparticles by using

$$\frac{\int_{\mathrm{Out}} \varepsilon(r)|E(r)|^2 d^3r}{\int_{\mathrm{Out+In}} \varepsilon(r)|E(r)|^2 d^3r} \quad (1)$$

where r is the position vector, $\varepsilon(r)$ is the local permittivity, $E(r)$ is the electric near field, Out and In are the outside and inside regions of the nanoparticle, respectively. For the ED resonance of the bare Si nanoparticle, the ratios are 0.75, while the ratios for the other resonances of both nanoparticles are 0.13–0.24. These values agree with the qualitative explanation mentioned above. From this discussion, it has been concluded that Si/SiO_2 nanoparticles can be nanostructures that are not affected by surrounding environment due to their high stability of the resonant wavelengths to the change of refractive indices of surrounding media.

We then calculated the electric near-field intensity enhancement for a Si/SiO_2 nanoparticle and a bare Si core. The near-field intensity enhancements of both particles were extracted from the outermost surface points where the field intensities are maximized. **Figure 6** shows the comparison of the near-field intensity enhancements for the Si/SiO_2 nanoparticle and the Si core. Similar to the forward scattering spectra, two peaks associated with MD and ED resonances are clearly observed in each spectrum. The bare Si core surface and Si/SiO_2 nanoparticle outermost surface show the

www.MaterialsViews.com

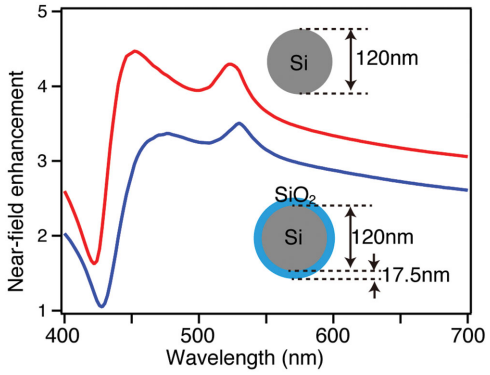

Figure 6. Comparison of near-field spectra on the outermost surfaces of the Si/SiO_2 nanoparticle (core diameter: 120 nm, shell thickness: 17.5 nm) and a bare Si core (core diameter: 120 nm).

field enhancements of approximately 4.3 and 3.5 at their MD resonances, respectively. The field enhancement for the Si/SiO_2 particle is smaller than that for the Si core; however, the difference of the enhancements between each MD resonance is only about 1.2 times. To realize higher enhancement, forming nanoantenna structures like dimmers is a potential way.[28]

In summary, we have fabricated core–shell nanoparticles comprising Si and SiO_2 through laser ablation and simple thermal oxidation. MDs and EDs were experimentally demonstrated to be strongly excited in Si/SiO_2 nanoparticles with the resonant wavelengths controlled by the variation of the core diameter through the thermal oxidation. Numerical calculations of scattering cross sections confirmed that shift of the resonant wavelengths of the particles was mainly derived from change of the core diameter. Besides the core size effect, refractive index of the surrounding medium was found to be a crucial factor to make the different optical resonant properties between bare Si and Si/SiO_2 nanoparticles. According to calculations for electric near-field intensity, Si/SiO_2 nanoparticles showed strong electric near-field enhancement comparable with that of Si nanoparticles, that have been regarded as a good electromagnetic field enhancer. Due to the simplicity of the fabrication procedure and the easy and precise control of the nanoparticle core diameter and resonant properties in a wide wavelength range, these systems are highly promising for the future use of Si-based nanostructures for field-enhanced spectroscopy, imaging, and metamaterials.

Experimental Section

Measurement of SiO_2 Thicknesses by an Ellipsometer: Si substrates were heated in an electric furnace stabilized at 800 °C under dry air conditions. At various oxidation times, the thicknesses of SiO_2 layers on Si substrates were determined using an ellipsometer (ELC-300, JASCO Corporation). In this measurement, a xenon lamp was used as a light source. The light was incident on the substrate with the incident angle of 70°, and then the reflected light from the substrate was detected with the wavelength range of 300–800 nm. For estimation of the thicknesses, optical constants in the database of ELC-300 were used.

Fabrication of Si Nanoparticles Through Laser Ablation and Si/SiO_2 Core–Shell Nanoparticles Through Thermal Oxidation: Si nanoparticles with spherical diameters of 100–200 nm were fabricated through laser ablation using a femtosecond laser (Hurricane, Spectra physics). For laser ablation, we used the experimental conditions described in previous studies.[5,11] A quartz glass plate was placed parallel to a Si wafer, and the distance between the quartz plate and wafer was fixed at 2 mm. The pulsed laser with a pulse width of 100 fs and a pulse energy of 1 mJ at a central wavelength of 800 nm was operated at a pulse repetition frequency of 1 kHz. The surface of the wafer was irradiated by the laser through the quartz plate. The spot diameter of the focused laser beam was ≈10 μm on the surface of the wafer. Ablated Si nanoparticles were collected on the quartz plate.

We themally oxidized the nanoparticles to form a SiO_2 shell around each Si nanoparticle. After the temperature of a furnace was stabilized at 800 °C, the nanoparticles were heated under dry air conditions in the furnace.

Dark-Field Forward Scattering Spectrosopy of Si/SiO_2 Core–Shell Nanoparticles: Fabricated core–shell structures were transported to a dark-field optical microscope (IX71, OLYMPUS), and then forward scattered light from the individual structures were investigated. To obtain the scattering spectra, a halogen lamp was used as a light source. The light was incident on the samples through a dark-field condenser (NA = 0.7–0.9), which led to the angle of light incidence in the range from 44° to 64° with respect to the normal to the quartz substrate. The forward scattered light was collected by an objective (SLCPlanFL, OLYMPUS, NA = 0.55, 40×), which provided the total angle for light collection of 67°. The collected light was detected by using a spectrometer (IsoPlane SCT320, Princeton Instruments) and an EMCCD (ProEM512, Princeton Instruments). By alternately repeating the thermal oxidation and dark-field observation for a same sample, scattering spectra from the same nanoparticle, but with different core–shell ratios were obtained.

Numerical and Analytical Calculations of the Scattering Spectra of Si/SiO_2 Core–Shell Nanoparticles: For numerical analysis of electromagnetic responses, we used the FEM software package COMSOL Multiphysics 4.4 (COMSOL Inc., Burlington, MA, USA). In the calculations, a single spherical core (Si)–shell (SiO_2) nanoparticle or a bare Si core in air were assumed. A plane wave was incident normally on the particle, and then forward scattered light was collected over the angle range of 33.5° from the incident axis. This detction range correspons to NA = 0.55 that was used in the experiment. For the calculation of the resonant wavelengths shown in Figure 5, we employed Mie theory for a bare Si and a core–shell nanoparticle.[29] Scattering cross sections of MD and ED resonances were individually obtained using Mie coefficients. Dielectric constants of Si and SiO_2 were taken from Palik.[30] Under these assumptions, we calculated the scattering cross sections, electric near-field distributions, and electric near-field enhancements for various values of Si core diameter and shell thickness.

Supporting Information

Supporting Information is available from the Wiley Online Library or from the author.

Acknowledgements

This work was partially sponsored by grant-in-aid for scientific research (25286030, 26630063, 26706006, 26107515), and JSPS Core-to-Core Program, A. Advanced Research Networks. This work was also supported in part by the Collaborative Research Project of Materials and Structures Laboratory, Tokyo Institute of Technology.

[1] P. Albella, R. A. de la Osa, F. Moreno, S. A. Maier, *ACS Photonics* **2014**, *1*, 524.
[2] P. Albella, M. A. Poyli, M. K. Schmidt, S. A. Maier, F. Moreno, J. J. Sáenz, J. Aizpurua, *J. Phys. Chem. C* **2013**, *117*, 13573.
[3] A. B. Evlyukhin, S. M. Novikov, U. Zywietz, R. L. Eriksen, C. Reinhardt, S. I. Bozhevolnyi, B. N. Chichkov, *Nano Lett.* **2012**, *12*, 3749.
[4] A. B. Evlyukhin, C. Reinhardt, A. Seidel, B. S. Luk'yanchuk, B. N. Chichkov, *Phys. Rev. B* **2010**, *82*, 045404.
[5] A. I. Kuznetsov, A. E. Miroshnichenko, Y. H. Fu, J. B. Zhang, B. Luk'yanchuk, *Sci. Rep.* **2012**, *2*, 492.
[6] D. L. Markovich, P. Ginzburg, A. K. Samusev, P. A. Belov, A. V. Zayats, *Opt. Express* **2014**, *22*, 10693.
[7] J. C. Ginn, I. Brener, D. W. Peters, J. R. Wendt, J. O. Stevens, P. F. Hines, L. I. Basilio, L. K. Warne, J. F. Ihlefeld, P. G. Clem, M. B. Sinclair, *Phys. Rev. Lett.* **2012**, *108*, 097402.
[8] A. García-Etxarri, R. Gómez-Medina, L. S. Froufe-Pérez, C. López, L. Chantada, F. Scheffold, J. Aizpurua, M. Nieto-Vesperinas, J. J. Sáenz, *Opt. Express* **2011**, *19*, 4815.
[9] R. Gómez-Medina, B. García-Cámara, I. Suárez-Lacalle, F. González, F. Moreno, M. Nieto-Vesperinas, J. J. Sáenz, *J. Nanophotonics* **2011**, *5*, 053512.
[10] RM. Bakker, D. Permyakov, Y. F. Yu, D. Markovich, R. Paniagua-Domínguez, L. Gonzaga, A. Samusev, Y. Kivshar, B. Luk'yanchuk, A. I. Kuznetsov, *Nano Lett.* **2015**, *15*, 2137.
[11] Y. H. Fu, A. I. Kuznetsov, A. E. Miroshnichenko, Y. F. Yu, B. Luk'yanchuk, *Nat. Commun.* **2013**, *4*, 1527.
[12] S. Person, M. Jain, Z. Lapin, J. J. Sáenz, G. Wicks, L. Novotny, *Nano Lett.* **2013**, *13*, 1806.
[13] B. Rolly, B. Stout, N. Bonod, *Opt. Express* **2012**, *20*, 20376.
[14] I. Staude, A. E. Miroshnichenko, M. Decker, N. T. Fofang, S. Liu, E. Gonzales, J. Dominguez, T. S. Luk, D. N. Neshev, I. Brener, Y. Kivshar, *ACS Nano* **2013**, *7*, 7824.
[15] A. E. Krasnok, A. E. Miroshnichenko, P. A. Belov, Y. S. Kivshar, *Opt. Express* **2012**, *20*, 20599.
[16] M. Kerker, D.-S. Wang, C. L. Giles, *J. Opt. Soc. Am.* **1983**, *73*, 765.
[17] A. B. Evlyukhin, C. Reinhardt, B. N. Chichkov, *Phys. Rev. B* **2011**, *84*, 235429.
[18] T. G. Habteyes, I. Staude, K. E. Chong, J. Dominguez, M. Decker, A. Miroshnichenko, Y. Kivshar, I. Brener, *ACS Photonics* **2014**, *1*, 794.
[19] U. Zywietz, A. B. Evlyukhin, C. Reinhardt, B. N. Chichkov, *Nat. Commun.* **2014**, *5*, 3402.
[20] W. Liu, A. E. Miroshnichenko, D. N. Neshev, Y. S. Kivshar, *ACS Nano* **2012**, *6*, 5489.
[21] R. R. Naraghi, S. Sukhov, A. Dogariu, *Opt. Lett.* **2015**, *40*, 585.
[22] W. Liu, J. Zhang, B. Lei, H. Ma, W. Xie, H. Hu, *Opt. Express* **2014**, *22*, 16178.
[23] J. Cazaux, *Nucl. Instrum. Methods B* **2006**, *244*, 307.
[24] Y. Lin, D. C. Joy, *Surf. Interface Anal.* **2005**, *37*, 895.
[25] W. Zhao, D. Ju, Y. Jiang, Q. Zhan, *Opt. Express* **2014**, *22*, 31277.
[26] B. García-Cámara, R. Gómez-Medina, J. J. Sáenz, B. Sepúlveda, *Opt. Express* **2013**, *21*, 23007.
[27] L. Shi, T. U. Tuzer, R. Fenollosa, F. Meseguer, *Adv. Mater.* **2012**, *24*, 5934.
[28] J. Yan, P. Liu, Z. Lin, H. Wang, H. Chen, C. Wang, G. Yang, *ACS Nano* **2015**, *9*, 2968.
[29] C. F. Bohren, D. R. Huffman, *Absorption and Scattering of Light by Small Particles*, Wiley Interscience, New York **1983**.
[30] E. D. Palik, *Handbook of Optical Constants of Solids*, Academic Press, Orlando **1985**.

Received: April 1, 2015
Revised: May 26, 2015
Published online: July 14, 2015

